Atmosphere-Ocean
Publication details, including instructions for authors and subscription information:
http://www.tandfonline.com/loi/tato20

The Changing Length of the Warming Period of the Annual Temperature Cycle in the High Latitudes Under Global Warming

John Bye [a] , Klaus Fraedrich [b] , Silke Schubert [b] & Xiuhua Zhu [b]
[a] School of Earth Sciences , The University of Melbourne , Victoria , 3010 , Australia
[b] KlimaCampus , University of Hamburg , Hamburg , Germany
Published online: 02 May 2013.

To cite this article: John Bye , Klaus Fraedrich , Silke Schubert & Xiuhua Zhu (2013) The Changing Length of the Warming Period of the Annual Temperature Cycle in the High Latitudes Under Global Warming, Atmosphere-Ocean, 51:3, 309-318, DOI: 10.1080/07055900.2013.793594

To link to this article: http://dx.doi.org/10.1080/07055900.2013.793594

The Changing Length of the Warming Period of the Annual Temperature Cycle in the High Latitudes Under Global Warming

John Bye[1,*], Klaus Fraedrich[2], Silke Schubert[2] and Xiuhua Zhu[2]

[1]*School of Earth Sciences, The University of Melbourne, Victoria 3010, Australia*
[2]*KlimaCampus, University of Hamburg, Hamburg, Germany*

[Original manuscript received 11 February 2012; accepted 8 March 2013]

ABSTRACT *The mechanism of climate change involves not only an increase in surface temperature but also an adjustment of the global seasons through changes in the timing of the annual temperature cycle. By locating the temperature extrema in monthly temperature records using Lagrangian interpolation in regions where a single maximum and minimum occurs, we define the warming period as the interval between the dates of the temperature minimum and the temperature maximum. The length and mid-point of the warming period are objective measures which can be computed from reanalysis data and from climate model predictions. We have used the 40-year reanalysis dataset from the European Centre for Medium-range Weather Forecasts (ERA40) and the European Centre Hamburg Model (ECHAM5) simulations to investigate the global distribution of the length and mid-point of the warming period for the present climate (1958–2001) and under global warming (Intergovernmental Panel on Climate Change, Fourth Assessment Report, Special Report on Emissions Scenarios; IPCC AR4 SRES A1B scenario) for the period 2157–2200.*

The results show that the warming period is remarkably uniform in the extratropical temperate latitudes, where it is about 22 days shorter than the cooling period in the ocean and of similar length on land. In the polar region, sharp geographical differences in the length and mid-point of the warming period occur over the ocean and over land which we attribute to the presence of sea ice. Under global warming, these differences are eroded and the temperate regime is extended poleward by about 10° in both hemispheres. This regime change is of particular importance to Canada, on which the discussion on global warming in high latitudes is focused.

RÉSUMÉ *[Traduit par la rédaction] Le mécanisme du changement climatique implique non seulement une augmentation de la température de surface mais aussi un ajustement des saisons dans leur ensemble par suite de changements dans le cycle annuel des températures. En repérant les extrêmes de température dans les registres météorologiques mensuels au moyen de l'interpolation lagrangienne dans les régions où se produisent un maximum et un minimum uniques, nous définissons la période de réchauffement comme l'intervalle entre la date du minimum et celle du maximum de température. La durée et le point médian de la période de réchauffement sont des mesures objectives pouvant être établies à partir de données de réanalyse et de prévisions de modèle climatique. Nous avons utilisé l'ensemble de données de réanalyse de 40 ans (ERA40) du Centre européen pour les prévisions météorologiques à moyen terme et les simulations du modèle de Hambourg (ECHAM5) du Centre européen pour étudier la distribution planétaire de la durée et du point médian de la période de réchauffement pour le climat présent (1958–2001) et suite au réchauffement planétaire (Groupe d'experts intergouvernemental sur l'évolution du climat, Quatrième Rapport d'évaluation, Rapport spécial sur les scénarios d'émissions; scénario IPCC AR4 SRES A1B) pour la période 2157–2200.*

Les résultats montrent que la période de réchauffement est remarquablement uniforme dans les latitudes de température extratropicale, où elle est d'environ 22 jours plus courte que la période de refroidissement sur l'océan et d'une durée similaire sur la terre. Dans la région polaire, des différences géographiques marquées sur la durée et le point médian de la période de réchauffement se produisent dans l'océan et sur la terre, différences que l'on attribue à la présence de glace de mer. Avec le réchauffement planétaire, ces différences s'érodent et le régime tempéré s'étend vers le pôle par environ 10° dans les deux hémisphères. Ce changement de régime est particulièrement important pour le Canada, auquel se rapporte la discussion sur le réchauffement planétaire dans les hautes latitudes.

KEYWORDS warming period definition; spring; global ERA40 climate data and ECHAM5 climate predictions; Canada; polar regions

[*]Corresponding author's email: jbye@unimelb.edu.au

1 Introduction

Canada is well known as a region of strong climate variability. In this paper our aim is not to discuss this variability in minutiae as this has been achieved already in many publications, for example, Turner and Gyakum (2010), but rather to examine why it occurs using a simple analysis of the annual cycle of global surface temperature. This analysis clearly indicates that seasonal change, as represented by changes in the length of the warming period of the cycle, is expected to be particularly significant in Canada under global warming, where it results primarily from changes in sea-ice concentrations and to a lesser extent from changes in the North Atlantic Ocean meridional circulation. Canada is especially vulnerable to these effects by virtue of its geography which comprises the Arctic Ocean and Hudson Bay to the north, Baffin Bay to the northeast, and the North Atlantic Ocean to the southeast. The results indicate a surprising hemispheric symmetry in high latitudinal change, but in the southern hemisphere its effect probably is of much lesser consequence.

For succinctness, we call the warming period of the annual cycle which occurs between the dates of minimum and maximum seasonal temperature, spring; similarly we call the cooling period which occurs between the dates of maximum and minimum seasonal temperature, autumn, and to avoid confusion with the conventional definitions, we *italicize* spring (and autumn) when referring to our results.

It follows that for climatology, which is considered in this paper, the sum of the *spring* length and the *autumn* length is exactly one year. In time series of several years, however, successive pairs of *springs* and *autumns* are not subject to this requirement. A question that may be posed is, what has happened to summer and winter? In the discussion below this question will not be addressed directly; however, the length of summer can be recovered as the interval between the *spring* mid-point and the following *autumn* mid-point, and the length of winter as the interval between the *autumn* mid-point and the following *spring* mid-point. Hence, our methodology provides a quantitative description of the lengths of the four seasons at all locations where one seasonal temperature maximum and one seasonal temperature minimum occur. Note that here the four seasons overlap in contrast to the conventional definition.

At other locations, predominately the tropics (Fig. 1), where multiple (seasonal) temperature extrema occur, the concept of spring and autumn is clearly not directly applicable.

In an era of climate change, our definition has an intrinsic advantage over the commonly used definitions of spring (March, April, and May in the northern hemisphere and September, October, and November in the southern hemisphere) and autumn (September, October, and November in the northern hemisphere and March, April, and May in the southern hemisphere) (Fowler & Fowler, 1964), which are relative to a fixed point in the calendar.

It is important at the outset to consider carefully the procedure for obtaining the dates of the seasonal temperature maximum and the seasonal temperature minimum. We use monthly mean data throughout because this provides a uniform dataset over land and ocean (where daily temperatures are not generally available), which is amenable to a simple three-point interpolation procedure to determine the extrema, the number of which may range from 2 to 12. An error analysis for the method is given in the Appendix, in which the two sources of error, the first arising from the use of monthly averaged data and the second from the interpolation of the monthly averaged data to obtain the dates of the seasonal temperature extrema, are assessed. It is concluded that for the approximately 40-year datasets used in the analyses, the expected errors of the climatological mean dates of the temperature extrema for locations with one temperature maximum and one temperature minimum are likely to be less than one or two days. The first part of this analysis is validated with observations of lag variability from 19 Australian stations (Alexander, Bye, & Smith, 2005). It is surprising that this straightforward method does not appear to have been used in the context of climate change in previous work.

One final general observation is that our analysis also differs from phenological studies of the onset of spring and of the length of the growing season, which apply temperature criteria to evaluate interannual variability under climate change (e.g., Chmielewski & Rotzer, 2001; Menzel & Fabian, 1999). This procedure is inherently geographically based, whereas the use of the timing of the seasons enables global comparisons of seasonal properties to be made, as is done in subsequent sections of this paper.

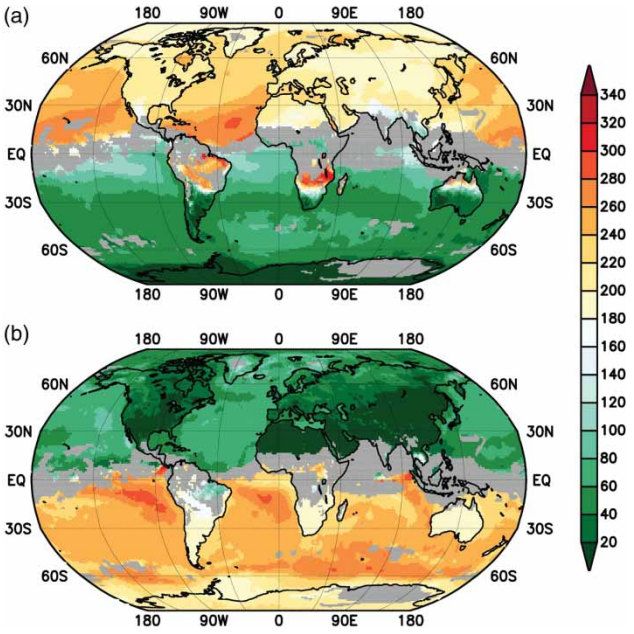

Fig. 1 (a) The day of global maximum temperature (t_{max}) for points with a single maximum. (b) The day of global minimum temperature (t_{min}) for points with a single minimum from the ERA40 dataset. Points with more than 1 maximum or minimum are shown in grey.

In Section 2, we present the details of the method of analysis of the monthly mean temperature fields and identify the gridded data sources. The climatology of the summer and winter temperature lags relative to the insolation cycle over the ocean and on land, based on the 40-year reanalysis dataset from the European Centre for Medium-range Weather Forecasts (ERA40), is discussed in Section 3 using, respectively, the days of temperature maximum and temperature minimum, from which the global distribution of the length of the warming period (*spring*) is derived. Section 4 is an extended discussion of changes in *spring* length and *spring* mid-point under global warming using the European Centre Hamburg Model (ECHAM5) simulations, which points out the dominance of polar changes, especially as they affect Canada. From this perspective, the causes of the changes are considered in Section 5 using the monthly mean temperature series at selected key points. The work is put into a wider context in Section 6.

2 Methodology and data sources

The results are based on an analysis of gridded monthly mean surface temperature data in which the extrema are searched by a Lagrangian interpolation over three consecutive months with the requirement that the extremum occurs within the three-month period (Bye, Fraedrich, Kirk, Schubert, & Zhu, 2011), and points which have one temperature maximum and one temperature minimum are selected. This procedure differs from the Fourier method, which is applied to resolve annual and sometimes semi-annual harmonics (Alexander et al., 2005; Li, Bye, Gallagher, & Cowan, 2012; Prescott & Collins, 1951; Stine, Huybers, & Fung, 2009; Yashayaev & Zveryaev, 2001). The one maximum and one minimum temperature fields enable the length and the mid-point of *spring* (or of *autumn*), and also the lag of the temperature maximum (minimum) relative to the summer maximum (winter minimum) in insolation in the subtropics, to be readily computed. These goals cannot be readily addressed using the Fourier method. In certain regions, notably the tropics, two or more temperature maxima and temperature minima occur in the annual cycle. These regions are identified but are only discussed where they are relevant to the extratropical climate, see Section 5.

For the observational climatology, we use the ERA40 (Uppala, 2003) dataset (1958–2001), which has a T106 (approximately 110 km resolution), and extract the fields of the globally defined surface temperature (TS). In contrast to sea surface temperature (SST), TS is the skin temperature at the interface, which in ice-covered regions is measured just above the ice.

For the predictions under global warming, we process the model results from the Fourth Assessment Report of the Intergovernmental Panel on Climate Change (IPCC AR4) A1B scenario obtained from the ECHAM5 model for the 1958–2001 period as a control for comparison with the observational data and the 2157–2200 period as a representation of global warming conditions. The resolution of the model results is T63 (approximately 180 km resolution), and the first period is a direct comparison with observations, whereas the second period occurs after the projected rise in CO_2 concentration to an equilibrium phase during which the CO_2 concentration is held constant at 720 ppm. In the ECHAM5 model the land surface parameters are specified (Hagemann, 2002). The model runs relevant to global warming are discussed in Hagemann, Arpe, and Roeckner (2006). An important feature of the analysis is that the summer and winter seasons are considered independently.

The method was applied to the average monthly temperatures at each grid point over the record period (1958–2001) of each dataset from which points with one maximum temperature (and one minimum temperature) were selected, and a mask was created over the remaining points, as illustrated in Fig. 1, and also to each grid point of the individual record years. The resulting four global fields: maximum temperature (T_{max}), minimum temperature (T_{min}), date (t_{max}) of T_{max}, and date (t_{min}) of T_{min}, were available for analysis. The ERA40 and ECHAM5 datasets provided, respectively, about 14000 and 5000 land point estimates and 30000 and 11000 sea point estimates for the four variables. Here we discuss the results for t_{max} and t_{min}, from which the summer lag, the winter lag, and the *spring* length and mid-point can be derived.

The summer lag (SL) is the time (in days) of the maximum temperature relative to the time of the peak in daily insolation in the subtropics, which occurs about 21 June in the northern hemisphere ($SL = t_{max} - 172$) and 22 December in the southern hemisphere ($SL = t_{max} + 9$). The winter lag (WL) is the time of minimum temperature relative to the time of the minimum in daily insolation, which occurs about 22 December in the northern hemisphere ($WL = t_{min} + 9$) and 21 June in the southern hemisphere ($WL = t_{min} - 172$). In both hemispheres the annual lag is $AL = (SL + WL)/2 = (t_{max} + t_{min})/2 - 81.5$. The interpretation of SL and WL is straightforward outside the tropics, which is the focus of this paper, although within the tropics many points also have only one maximum and minimum temperature (Fig. 1).

The *spring* length is the warming period of the annual cycle ($SP = t_{max} - t_{min}$, $t_{max} > t_{min}$; $SP = t_{max} - t_{min} + 365$, $t_{max} < t_{min}$), and the *autumn* length is the cooling period ($AU = t_{min} - t_{max}$, $t_{min} > t_{max}$; $AU = t_{min} - t_{max} + 365$, $t_{min} < t_{max}$). For climatologically averaged data, $SP + AU = 365$, and the *spring* mid-points (MP) in the northern hemisphere and the southern hemisphere are, respectively, $MP = (t_{max} + t_{min})/2$, and $MP = (t_{max} + t_{min})/2 + 182.5$, which occur after the spring equinox by the annual lag (AL). Similarly, the *autumn* mid-point lags the autumn equinox by AL, from which it follows that the lengths of winter and summer are exactly 182.5 days (one-half year). Hence, the annual lag is truly "the lag of the seasons."

3 Climatology of summer and winter lags and *spring* length

a *Global Means*

The global mean averages (over all years and all grid points) of summer lag, winter lag, and *spring* length and *spring*

Table 1. The mean and standard deviation of summer and winter lags, the annual lag, and the length and mid-point of *spring* (days) over the ocean and land excluding the tropics from the ERA40 dataset and the ECHAM5 model. Italics denote temporal averaging only, see text.

		Ocean	Land	Ocean	Land
		Summer lag		Winter lag	
ERA40	1958–2001	61 ± 14	26 ± 11	72 ± 16	26 ± 12
ERA40	1958–2001	*61 ± 1*	*26 ± 1*	*71 ± 2*	*24 ± 3*
ECHAM5	1958–2001	65 ± 14	27 ± 11	77 ± 16	26 ± 10
ECHAM5	2157–2200	67 ± 12	29 ± 12	81 ± 14	29 ± 12
		Annual lag		*Spring* length	
ERA40	1958–2001	66.5	26	171.5	182.5
ECHAM5	1958–2001	71	26.5	170.5	183.5
ECHAM5	2157–2200	74	29	168.5	182.5
		Spring mid-point (northern hemisphere)		*Spring* mid-point (southern hemisphere)	
ERA40	1958–2001	148	107.5	330.5	290
ECHAM5	1958–2001	152.5	108	335	290.5
ECHAM5	2157–2200	155.5	110.5	338	293

mid-point, excluding the tropics, are shown in Table 1 for land and ocean. For the ERA40 dataset, on combining the summer and winter values, the annual lag over the ocean (66 ± 15 d) is greater than the estimate (56 ± 11 d) from Stine et al. (2009) and on land (26 ± 11 d) is less than their estimate (29 ± 6 d). We note that our spatial resolution is much finer than the $5° \times 5°$ spatial averaging used in Stine et al. (2009) in which the coastline is represented at a lower resolution. The standard deviations in the ERA40 results are mainly caused by spatial variability, as is apparent in Fig. 1, rather than temporal variability. This conclusion was tested by computing the standard deviation and mean of lag at each grid point at which the climatological mean temperature record had a single temperature maximum and then averaging over all these grid points (Table 1). The standard deviations of the temporal lag variability clearly are less than for the total variability by an order of magnitude, and there are also differences in the mean lags, which arise from the omission of some grid points in the temporal averaging resulting from the occurrence of multiple maximum temperatures in the climatological mean record.

The mean length of *spring* in the ocean is about 22 days shorter than that of *autumn*, which for the climatologically averaged data has an anomaly of opposite sign to *spring*. This is brought about by the retention of heat in the stable water column in autumn in the extratropical ocean. On land, *spring* (and a*utumn*) are of approximately the same length (Table 1). The mid-point of *spring* occurs about 40 days later in the ocean than on land. The smaller mean winter lags on land and over the ocean for the temporal variability relative to the total variability occur primarily because most of the omitted grid points are in the near-tropical region.

The ECHAM5 modelled lags for the observational period are longer than the ERA40 observational lags by about 5 days in the ocean, which suggests that the heat exchange cycle with the deeper layers of the ocean may be underestimated in the model (Table 1). There is also a zero seasonal lag anomaly on land in agreement with the ERA40 data.

b *Global Fields of Lag*

In the oceans, the most striking subtropical features in the ERA40 data are the tongues of higher lag in the t_{max} and t_{min} fields (Fig. 1), which originate in the tropics and appear to coincide with the trade wind circulations. Our seasonal results show that these tongues, which previously have been identified in the AL (Li et al., 2012), are present throughout the year and are particularly evident in the southern hemisphere. On the basis of a Langevin model for heat exchange between the atmosphere and the ocean (Bye et al. 2011; Frankignoul, Czaja, & L'Heveder, 1998), the maxima in lag indicate regions of minimum thermal feedback, which characterize the atmospheric general circulation in low latitudes as discussed in Li et al. (2012) in which it is also suggested that a second region of increased lags in the vicinity of the confluence of the warm Agulhas Current and the Antarctic Circumpolar Current (Fig. 1) may arise from a reduction of feedback because of mesoscale eddy formation. There are also isolated outcrops of double pairs of extrema between 45°S and 60°S to the west of Australia and between New Zealand and South America which coincide with the positions of maxima in the semi-annual oscillation (SAO) in meridional temperature gradient between 50°S and 65°S, which is a result of the differential heating and cooling of the ocean relative to Antarctica (Simmonds & Jones, 1998; Walland & Simmonds, 1999).

On land, the extratropical distributions of t_{max} and t_{min} are rather featureless, and on the high Antarctic plateau, the double pairs of extrema identify the world's coldest winter region (Fig. 1b).

c *Global Field of Spring Length*

The global distribution of the length of *spring* (Fig. 2a), notwithstanding the differences in mean *spring* length over the land and ocean, shows many regions where the length of *spring* varies continuously over the coast, notably between the North Atlantic Ocean and southern Europe and off eastern South America and to some extent Australia. In the ocean, the shortest *springs* occur in the temperate latitudes where *spring* may be up to three months shorter than *autumn*, whereas in the Tropics the situation is reversed and *autumn* may be up to three months shorter than *spring*. A notable feature in the subpolar seas is the "bullseye" of longer *springs* in Hudson Bay of about two months relative to the North Atlantic Ocean. These regions of longer *springs* also occur in Baffin Bay and the Kara Sea and are mirrored in the high latitude region of the Southern Ocean (Fig. 2a).

In the temperate land masses, the length of *spring* has little variability, either with latitude or longitude (Fig. 2a), the small meridional variability being evident in the zonal mean fields (Fig. 3a). It is also remarkable that the zonal mean *spring* lengths are almost symmetrical between the two hemispheres

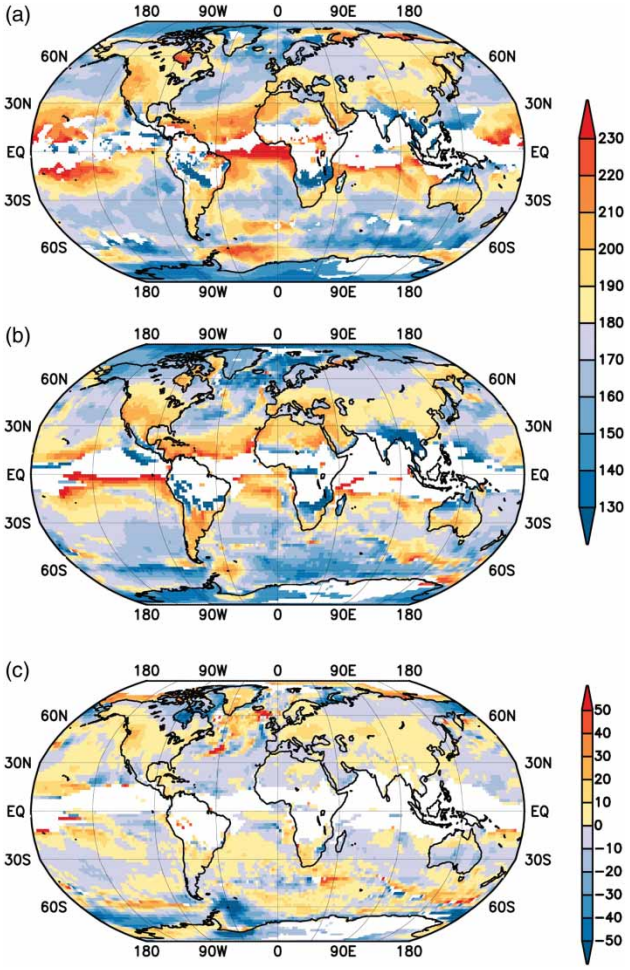

Fig. 2 (a) The global length of spring in 1958–2001 from the ERA40 dataset. (b) The global length of *spring* in 1958–2001 from the ECHAM5 model. (c) The change in the global length of *spring* between 1958–2001 and 2157–2200 from the ECHAM5 model. Points with more than 1 maximum or minimum are shown in white.

(notwithstanding the antithetical geography) with the property in each instance that *spring* and *autumn* are of about the same length as the Tropics are crossed (Fig. 3a). The *spring* MP on the Tropics (Fig. 3b), however, is about 40 days later in the ocean than on land, and since the MP is almost constant throughout the temperate latitude band, this offset is very similar to the difference in the global means, excluding the Tropics, of the ocean and land lags of 40.5 days (Table 1). In summary, the temperate *spring* pattern is remarkably simple. At higher latitudes around 60°, however, the two maxima in oceanic SP mentioned above are clearly evident in the zonal mean distributions, together with a decrease in MP poleward of 60°N.

The ECHAM5 SP distributions for the observational period are in general agreement with the ERA40 distributions (Fig. 2b), hence predicted changes under global warming can be usefully examined, and the simulations offer a good opportunity for the investigation of the physical processes which determine lag, SP, and MP.

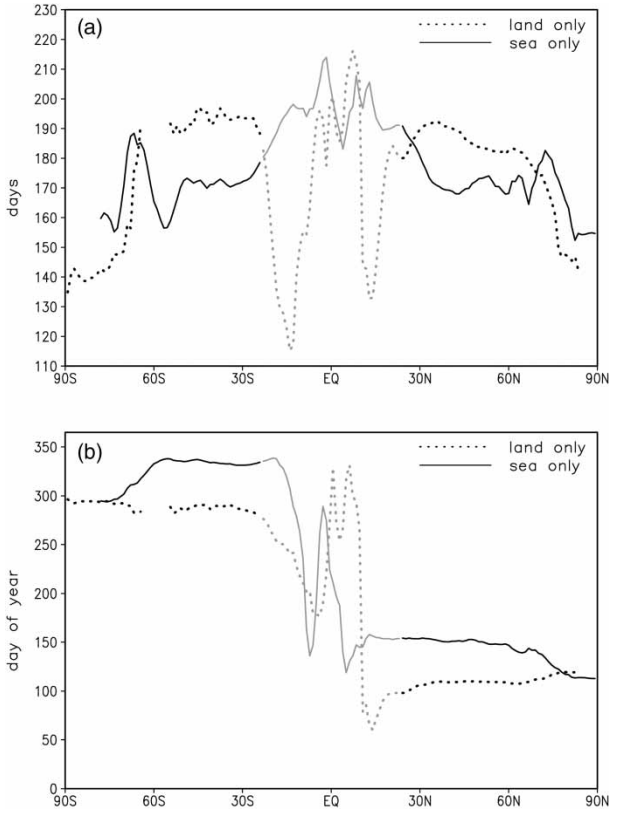

Fig. 3 (a) Zonal mean *spring* length (days) on land and in the ocean in 1958–2001 from the ERA40 dataset. (b) Zonal mean *spring* mid-point (day of year) on land and in the ocean in 1958–2001 from the ERA40 dataset. Tropical zonal mean values (not discussed in the text) are shown in light grey.

4 Lag variability and changes in *spring* length under global warming

a *Global Mean Changes*

The ECHAM5 model indicates that in the IPCC AR4 A1B scenario, by 2157–2200 there is a greater increase in global mean WL than SL, and hence *spring*, which is shorter than autumn by approximately 24 days over the ocean, becomes even shorter (by 28 days) under global warming. On land, the two seasons have about the same length throughout, and the mean of the standard deviations of WL and SL remain almost constant, but by 2157–2200 the predicted standard deviations of SL and WL have become similar (Table 1). From general reasoning, an increase in lag under global warming is quite consistent with the greater trapping of heat by the higher concentrations of greenhouse gases. The larger change in WL than in SL suggests that this increase is primarily a result of polar factors. Note that the predicted changes in mean lag under global warming are significant because they are greater than the temporal mean standard deviations in lag (Table 1). We have selected 2157–2200 as the period of comparison because the effects of global warming have become clear by this period; they are also evident for the earlier period, 2057–2100.

b *Global Field of Changes in Spring Length*

Under global warming large regional differences in the anomalies in *spring* length occur which are continuous over land and ocean (Fig. 2c). In particular, temperate Eurasia and North America develop extensive regions of positive (long) *spring* anomaly. These anomalies, which are also found in the temperate oceans of the southern hemisphere and in the southerly regions of the continents, are a result of an increase in SL, which arises from the expansion of the tropical belt under global warming (Li et al., 2012). The increases in SL are of similar magnitude to the increases in the lag of maximum temperature observed in southern Australia between 1900 and 2000 (Alexander et al., 2005). Compensatory short *spring* anomalies occur in the subtropical oceans and in the Sahara and central Australia.

The predicted changes in SP (Fig. 2c), however, are largest in the polar region. This is especially apparent in the Canadian Arctic. Here an intense negative SP anomaly occurs in Hudson Bay and Baffin Bay, which compensates for the present day positive SP anomalies in these regions, and also extends into eastern Canada. A similar anomaly is centred in the Kara Sea, which extends its influence over Siberia. In the Arctic Ocean, Greenland, and the North Atlantic Ocean, on the other hand, positive SP anomalies occur which tend to compensate for the present day negative anomalies. In the southern hemisphere the decreases in SP of about 30 days in the subpolar regions of the Southern Ocean are partially compensated for by increases further north in the Antarctic Circumpolar Current. In the temperate latitudes, the changes in the length of *spring* over both land and ocean are generally less than 10 days (Fig. 2c).

The zonal mean changes (Figs 4a and 4b) summarize three main conclusions. First, the changes in SP in temperate latitudes are small both on land and in the oceans. Second, in the polar region around 60°, there are spikes of negative SP anomaly, which compensate for the maxima in SP in the contemporary climate and essentially extend the temperate regions of almost uniform SP poleward by about 10°. Third, poleward of 60°, the *spring* MP increases steeply in the ocean, which tends to compensate for the present day poleward decrease in MP (Fig. 4b) and is also consistent with the increase in global mean lag (Table 1) being a result of high latitude oceanic processes.

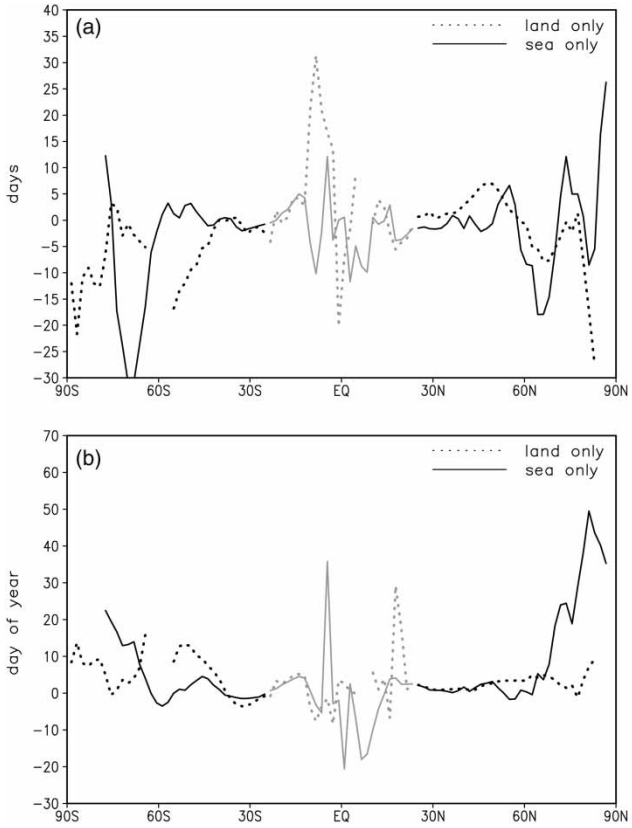

Fig. 4 (a) Change in zonal mean *spring* length (days) between 1958–2001 and 2157–2200 from the ECHAM5 model. (b) Change in zonal mean *spring* mid-point (day of year) between 1958–2001 and 2157–2200 from the ECHAM5 model. Tropical zonal mean values (not discussed in the text) are shown in light grey.

5 Selected global warming changes in monthly mean temperature

The changes in SP outlined above highlight a few key regions where it is useful to examine the corresponding monthly mean temperature distributions.

The clearest change in lag occurs in the high Arctic, where, for example, at 81°N, 156°W (Fig. 5b) during the summer an almost constant surface temperature of just less than 0°C occurs in 2157–2200 as a result of low salinity surface water produced by ice melt, which is neatly identified by the double pairs of extrema that occur in the Arctic Ocean (Fig. 2c). In winter, the minimum temperature has risen by about 12°C. In the Antarctic at 71°S, 101°E, the seasonal pattern is almost unchanged although by 2157–2200 the winter temperature has increased by about 6°C and the summer temperature by about 3°C (Fig. 5a).

Under global warming, therefore, the polar monthly mean temperature signals in the maritime Arctic and the continental Antarctic display a beautiful "sunny-side up" antisymmetry in which a plateau of maximum temperature occurs in the Arctic in summer, and in the Antarctic a plateau of minimum temperature occurs in the winter.

Major seasonal changes are also found in the subpolar region. In Canada, much shorter *springs* occur at 60°N, 85°W in Hudson Bay (Fig. 5d) because of extended autumnal conditions with much less sea ice, which give rise to later winters. Similar sea-ice changes are also predicted for Baffin Bay and the Kara Sea. In the outer Weddell Sea in the Southern Ocean, for example, at 61°S, 43°W (Fig. 5e), much shorter *springs* are also a result of the later winters, which arise because of ice-free conditions when TS is greater than −2°C.

Three of the above four examples are clearly controlled by changes in the sea-ice fields, which result from an overall continental temperature rise, which according to the ECHAM5

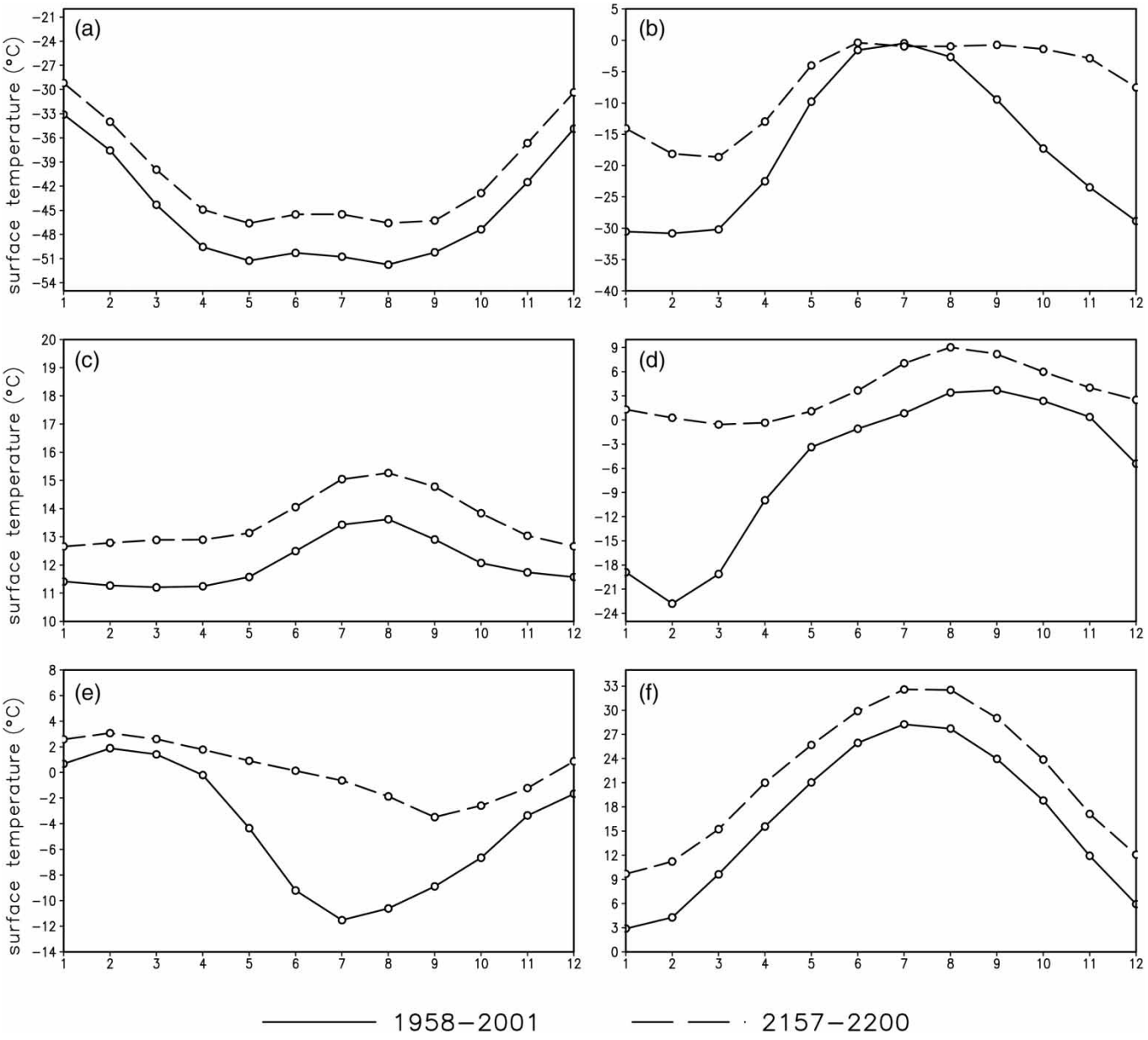

Fig. 5 Mean monthly surface temperatures for the periods 1958–2001 and 2157–2200 from the ECHAM5 model: (a) Antarctic plateau (72°S, 101°E), (b) Arctic Ocean (81°N, 156°W), (c) North Atlantic Ocean (60°N, 11°E), (d) Hudson Bay (60°N, 85°W), (e) Southern Ocean (61°S, 43°W), and (f) Central China (30°N, 115°E). The numbers 1–12 indicate January–December.

model is of very similar magnitude in two environments as distinct as 72°S, 101°E in Antarctica (Fig. 5a) and 30°N, 115°E in central China (Fig. 5f).

An ice-free oceanic response in the northern North Atlantic Ocean relevant to Canada also occurs, for example, at 60°N, 11°E, *spring* becomes longer because winter occurs earlier (Fig. 5c). This change appears to be caused by a reduction in the importance of the meridional circulation as a bringer of late season warmth to the higher latitudes, as is suggested by the reduction in magnitude of the oceanic warming in comparison with the continental warming in Central China.

In summary, under global warming, Canada is predicted to be affected by three centres of seasonal change, as gauged by SP and *spring* MP. First, in the high Arctic, longer *springs* give rise to later summers (Fig. 5b). Second, the reduction in sea ice in Hudson Bay and Baffin Bay gives rise to later winters and shorter *springs* (Fig. 5d). Third, the reduction in the penetration of the meridional circulation in the northern North Atlantic Ocean produces earlier winters and longer *springs* (Fig. 5c).

In the southern hemisphere, these three predicted changes, especially the second change in the outer Weddell Sea in which later winters and shorter *springs* occur, are also apparent. In the Ross Sea and the inner Weddell Sea, the changes

appear to be of similar origin to those in the high Arctic in which longer *springs* and later summers occur, and in the Southern Ocean earlier winters and longer *springs* are produced by a reduction in the interaction of warmer subtropical gyral water with the cooler water mass of the Antarctic Circumpolar Current (Fig. 4a).

The predicted seasonal change responses in the ice-free oceans neighbouring the polar seas in both hemispheres, therefore, are consistent with a reduction in interaction between the two regions under global warming.

6 Discussion

Spring is welcomed by all cultures (for example, "sweet spring, full of sweet days and roses" *Virtue. verse 3, line 1:* George Herbert 1591–1633). Our results indeed show that the zonal means of SP and *spring* MP on land and in the ocean, which are the basic measures of the warming period, are almost constant in the temperate latitudes and have almost symmetrical hemispheric distributions (Figs 3a and 3b). This symmetry even extends poleward into the icy environment, which imparts a meridional structure to the two spring properties. Under global warming this high latitude structure is likely to be eroded, effectively extending the temperate zone poleward by up to 10°.

The causes of the seasonal structure in the temperate regions are that on the land the lag is basically determined by the ground delay imparted to the radiation signal with minor adjustments resulting from the vegetation cover, whereas in the ocean the lag is determined by the slower response of the surface ocean layers to the radiation signal, which is seasonally asymmetric giving rise to a large negative SP anomaly in which autumn is longer than spring by about 22 days

In this study we have used the ECHAM5 climate model. The equilibrium climate sensitivity (the global mean surface air temperature change after adjustment to a doubling in atmospheric CO_2 concentration) is 3.4°C, which is in the mid-range of 19 AR4 climate models, which have an average equilibrium climate sensitivity of 3.2°C. The transient climate response (the annual mean temperature change over a 20-year period centred at the time of CO_2 doubling of 1% per year) of ECHAM5 is 2.2°C, which is somewhat greater than the mean value for the 19 climate models of 1.8°C (IPCC, 2007, Table 8.2). This bias appears to be reflected in the greater oceanic lag in the ECHAM5 model relative to the ERA40 observations (see Section 3a). Comparison of the annual mean and standard deviation of the global fields of surface temperature of AR4 models is given in IPCC (2013). As mentioned in Section 4b, the temperate regime is abruptly terminated on each tropic (Fig. 3a) where the SP anomaly both on land and in the ocean is almost zero, although the MP is unchanged (Fig. 3b). This change is primarily a result of the difference in the response of the surface ocean layer in the tropical region of reduced thermal feedback where *autumn* becomes shorter than *spring* (i.e., t_{max} increases relative to t_{min} (Fig. 1)).

The changes in SP and *spring* MP in the polar region relevant to Canada under global warming were presented in Section 5. Interannual and interdecadal climate variability are not the main focus of this paper, but a full discussion is available from the yearly fields of minimum and maximum temperature (T_{min}, T_{max}), winter and summer lag (WL, SL), and *spring* length (SP) and mid-point (MP) derived in the analysis. The random variability of T_{min}, T_{max}, WL, and SL obtained from the ERA40 dataset, however, has been discussed on a global scale in Bye et al. (2011), in which it was shown that random walks of about 30 years in length occur. The same method can be applied on a regional scale.

For Canada, the standard deviations of WL and SL are, respectively, about 15 days and 8 days (Bye and Fraedrich, unpublished manuscript). Hence, assuming that WL and SL are only weakly correlated and applying the formula for the expected maximum excursion in a random walk of Feller (1962) used in Bye et al. (2011), assuming a random walk length of 30 years, we obtain an expected maximum excursion in SP of 74 days, which is about 40% of the mean SP of 190 days (Fig. 3a), and similarly the expected maximum excursion of MP is 37 days. These statistics appear to be consistent with observed Canadian climate variability (e.g., Szeto, 2008). The variability of all four seasons for any chosen region can be thoroughly investigated using this methodology.

The variability of the annual lag in the ocean, determined from the updated Hadley Centre Global Sea Ice and Sea Surface Temperature (SST) (HadISST) dataset (Rayner et al., 2003), has also been investigated in an independent analysis by Li et al. (2012) who fitted an annual Fourier mode. It was found that the mean annual lag fields were similar to the oceanic AL field obtained from Figs 1a and 1b and also that significant oceanic lag anomalies occurred between the two consecutive periods (1976–1990 and 1991–2005), which were also simulated using the Scenario A2 run from the Commonwealth Scientific and Industrial Research Organisation (CSIRO) Mk3.5 T63 climate model (Gordon et al., 2002).

Acknowledgements

The work presented in this paper was made possible by a computer program for analyzing the lag provided by Edilbert Kirk (KlimaCampus, The University of Hamburg). JB gratefully acknowledges support given by Integrated Climate System Analysis and Prediction (CliSAP), Hamburg, in two invited visits to the KlimaCampus, and KF acknowledges support by the Max Planck Society, and John Boland is especially thanked for advice and discussions. The paper was completed whilst JB held a Fellowship at the Hanse Institute for Advanced Study in Delmenhorst, Germany, during the first six months of 2013. The reviewers and the Associate Editor are also thanked for their useful comments, which have greatly improved the presentation of our results.

Appendix A: Error analysis for the Lagrangian interpolation of monthly mean data

There are two factors which are relevant in obtaining the estimates of the dates of maximum and minimum temperature:

(1) The choice of the scale of averaging over which the temperatures are obtained. The aim is to select a time scale which is long enough to average over the synoptic variability but short enough to retain the seasonal variability.
(2) The choice of the interpolation procedure to determine the central point in the seasonal temperature.

We consider each in turn using the simple model,

$$T = \cos(\sigma t - \psi) + A\cos n\sigma t, \tag{A1}$$

in which T is a normalized temperature of unit amplitude which represents the seasonal temperature signal and is assumed to be locally of annual harmonic form, where σ is the annual frequency, and A is the relative amplitude of a short period temperature variability also assumed for convenience to be of harmonic form with a frequency, $n\sigma = 2\pi/T_w$ where T_w is the period of the variability. In Eq. (A1) the seasonal temperature signal has a maximum at $t_{\max} = \psi/\sigma$.

We assume that the data are available on an average period of Δ. Then on integrating Eq. (A1) over the interval $(t - \Delta/2, t + \Delta/2)$ we obtain,

$$< T > = \left[\frac{\sin 1/2\Delta\sigma}{(1/2\Delta\sigma)}\right]\cos(\sigma t - \psi) + A\left[\frac{\sin(n/2\Delta\sigma)}{(n/2\Delta\sigma)}\right]\cos n\sigma t, \tag{A2}$$

where $< T > = 1/\Delta\int_{t-\Delta/2}^{t+\Delta/2} T\,dt$. On differentiating Eq. (A2) with respect to time we find that at a maximum of $<T>$,

$$-\sigma\sin(\sigma t - \psi) + \frac{d\varepsilon(t)}{dt} = 0, \tag{A3}$$

where $\varepsilon(t) = A[1/2\sigma\Delta/\sin(1/2\sigma\Delta)]\ [\sin(n/2\Delta\sigma)/(n/2\Delta\sigma)]\ \cos n\sigma t$, in which for monthly averages, $\Delta = \pi/(6\sigma)$, hence $\sigma\Delta = \pi/6$ and $1/2\Delta\sigma/\sin(1/2\ \Delta\sigma) = 1.012$.

For $\varepsilon(t) \to 0$, the uncertainty in the estimate of $t_{\max}$,

$$t'_{\max} = \frac{1}{\sigma^2}\frac{d\varepsilon(t)}{dt}. \tag{A4}$$

This variability arises from the harmonics in the seasonal cycle, which have a Nyquist frequency, $n_0 = 1/2\ \sigma/\Delta$. On assuming a root-mean-square estimate for the product $(\sin n/2\Delta\sigma)\ (\cos n\sigma t)$ of $1/\sqrt{2}$, and a cycle of averaged data of frequency, n_0, and evaluating Eq. (A4) we obtain,

$$\mathrm{sd}\,(t'_{\max}) \approx \frac{1}{\sqrt{2}} A\,T_w(\Delta\sigma)^{-2}, \tag{A5}$$

where sd is the standard deviation. On evaluating Eq. (A5) assuming that $T_w = 5$ days and $A = 0.5$, which are representative of the synoptic variability, we obtain, $\mathrm{sd}(t'_{\max}) = 7$ days. This heuristic estimate is consistent with observations of the standard deviation of the lags of maximum temperature in 19 Australian stations obtained using a Fourier window technique, for which the mean value was 7.3 days (Alexander et al., 2005). It is interesting that the observational estimate of the standard deviation in the date of the maximum seasonal temperature and the theoretical estimate Eq. (A5), $\mathrm{sd}(t'_{\max}) \approx T_w$, are both similar to the period of the synoptic variability.

Over m determinations the standard deviation would be expected to be reduced by the factor, $\sqrt{m}$, hence for $m = 40$, the predicted standard deviation of $t_{\max}$ is about 1 day.

Hence, we conclude that the use of monthly averaging introduces a very small error in estimates of $t_{\max}$, especially if several determinations are averaged. In practice, however, monthly averages are only available at monthly intervals, and it is necessary to interpolate to estimate $(t_{\max})$. On assuming that $\varepsilon\,(t) = 0$, we estimate $t_{\max}$ by $t^{\mathrm{L}}_{\max}$, which is derived from a Lagrangian interpolation over three consecutive months with the caveat that $t^{\mathrm{L}}_{\max}$ occurs within this period.

On assuming that

$$< T > = a\,t^2 + b\,t + c, \tag{A6}$$

the maximum in $<T>$ occurs at,

$$t^{\mathrm{L}}_{\max} = \frac{-b}{2a}. \tag{A7}$$

On now applying the triad $(t = -1/12,\ t = 0,\ t = 1/12)$ relative to the central month $(t = 0)$ and evaluating a, b, and c in Eq. (A6) using Eq. (A2) with $A = 0$, we obtain,

$$t^{\mathrm{L}}_{\max} = \frac{1/24\sin\pi/6}{(1 - \cos\pi/6)}\tan\psi. \tag{A8}$$

For monthly averaging Eq. (A8) yields $t^{\mathrm{L}}_{\max} = 0.155\tan\psi$, whereas $t_{\max} = 0.159\psi$. Hence, for $\psi = 0$, Lagrangian interpolation is precise; however, if $t^{\mathrm{L}}_{\max}$ occurs at the limits of acceptance, $t = \pm 1/12$ (0.083), on substituting in Eq. (A8) we obtain $\psi = \pm 0.492$ from which $t_{\max} = \pm 0.078$. Hence, if $\psi > 0$, $t_{\max}$ is overestimated by $1.7 = 30.2–28.5$ days, and if $\psi < 0$, $t_{\max}$ is underestimated by 1.7 days. This small uncertainty in the date of the maximum temperature is much less than that obtained from just choosing the month with the maximum average temperature for which the maximum error in $t_{\max}$ is ± 15.2 days.

The Lagrangian interpolation was applied successively over each of the 12 monthly triads (December–February to November–January) of the average monthly temperature record to determine all the extrema.

In conclusion, this analysis suggests that the total errors in the timing of the summer $(t_{\max})$ and also the winter $(t_{\min})$ seasonal extrema for a 40-year climatology are likely to be less than one or two days.

References

Alexander, B. M., Bye, J. A. T., & Smith, I. N. (2005). Australian summer maximum temperature lags. *Australian Meteorological Magazine*, *54*, 103–113.

Bye, J. A. T., Fraedrich, K., Kirk, E., Schubert, S., & Zhu, X. (2011). Random walk lengths of about 30 years in global climate. *Geophysical Research Letters*, *38*, L05806. doi:10.1029/2010GL0463 33.2011

Chmielewski, F. M., & Rotzer, T. (2001). Response of tree phenology to climate change across Europe. *Agricultural and Forest Meteorology*, *108*, 101–112.

Feller, W. (1962). *An introduction to probability theory and its applications*. New York: John Wiley.

Fowler, H. W., & Fowler, F. G. (Eds.). (1964). *The concise Oxford dictionary of current English* (5th ed.). New York: Oxford University Press.

Frankignoul, C., Czaja, A., & L'Heveder, B. (1998). Air-sea feedback in the North Atlantic and surface boundary conditions for ocean models. *Journal of Climate*, *11*, 2310–2324.

Gordon, H. B., Rotstayn, L. D., McGregor, J. L., Dix, M. R., Kowalizyk, E. A., O'Farrell, S. P., … Elliot, T. I. (2002). *The CSIRO Mk3 climate system model*. CSIRO Atmospheric Research Technical Paper 60. Aspendale, Australia: CSIRO.

Hagemann, S. (2002). *An improved land dataset for global and regional climate models*. Report 386. Max-Planck-Institut fur Meteorologie, Hamburg.

Hagemann, S., Arpe, K., & Roeckner, E. (2006). Evaluation of the hydrological cycle in the ECHAM5 model. *Journal of Climate*, *19*, 3810–3827.

IPCC (Intergovernmental Panel on Climate Change). (2007). *Climate Change 2007: The physical science basis. Contribution of Working Group I to the Fourth Assessment Report of the Intergovernmental Panel on Climate Change*. Cambridge: Cambridge University Press.

IPCC (Intergovernmental Panel on Climate Change). (2013). *IPCC Fourth Assessment Report, Climate Change 2007* (AR4 WG1 Figures Chapter 8). Retrieved from http://www.ipcc.ch/publications_and_data/publications_and_data_figures_and_tables.shtml

Li, C-L., Bye, J. A. T., Gallagher, S. J., & Cowan, T. (2012). Annual sea surface temperature lag as an indicator of regional climate variability. *International Journal of Climatology*. doi:10.1002/joc.3587

Menzel, A., & Fabian, P. (1999). Growing season extended in Europe. *Nature*, *397*, 659.

Prescott, J., & Collins, J. (1951). The lag of temperature behind solar radiation. *Quarterly Journal of the Royal Meteorological Society*, *77*, 121–126.

Rayner, N. A., Parker, D. E., Horton, E. B., Folland, C. K., Alexander, L. V., Rowell, D. P., … Kaplan, A. (2003). Global analyses of sea surface temperature, sea ice, and night marine air temperature since the later nineteenth century. *Journal of Geophysical Research*, *108*(D14), 4407. doi:10.1029/2002JD002670

Simmonds, I., & Jones, D. A. (1998). The mean structure and temporal variability of the semiannual oscillation in the southern extratropics. *International Journal of Climatology*, *18*, 473–504.

Stine, A. R., Huybers, P., & Fung, I. Y. (2009). Changes in the phase of the annual cycle of surface temperature. *Nature*, *457*, 435–441.

Szeto, K. K. (2008). On the extreme variability and change of cold-season temperatures in northwest Canada. *Journal of Climate*, *21*, 94–113.

Turner, J. K., & Gyakum, J. R. (2010). Trends in Canadian surface temperature variability in the context of climate change. *Atmosphere-Ocean*, *48*, 147–162. doi:10.103137/AO1102.2010

Uppala, S. (2003). World Data Center for Climate, Hamburg. Metadata for CERA experiment ERA40_SFC00_MM [Surface Data, monthly means] CERA-DB "ERA40_SFC00_MM," Retrieved from http://cera-www.dkrz.de/WDCC/ui/Compact.jsp?acronym=ERA40_SFC00_MM

Walland, D., & Simmonds, I. (1999). Baroclinicity, meridional temperature gradients, and the Southern Oscillation. *Journal of Climate*, *12*, 3376–3382.

Yashayaev, I. M., & Zveryaev, I. I. (2001). Climate of the seasonal cycle in the North Pacific and the North Atlantic Oceans. *International Journal of Climatology*, *21*, 401–417.